On the bootstrap current in the TJ-II stellarator

Katia Camacho & Julio J. Martinell

Published online: 17 Apr 2017.

Submit your article to this journal ⬀

View related articles ⬀

View Crossmark data ⬀

Taylor & Francis
Taylor & Francis Group

Check for updates

On the bootstrap current in the TJ-II stellarator

Katia Camacho and Julio J. Martinell

Instituto de Ciencias Nucleares, UNAM, México D.F., Mexico

ABSTRACT

Bootstrap current in stellarators is usually very small since they operate solely with the magnetic confinement provided by the external currents. Since plasma pressure gradients are always present, the bootstrap current is always finite, but the magnetic design can be optimized to minimize it. In the heliac configuration, there is no optimization and therefore it is important to estimate the actual bootstrap current generated by given pressure profiles. Here, we use the configuration of the TJ-II heliac to calculate the bootstrap current for various density regimes using the kinetic code DKES. We compute the mono-energetic transport coefficients D_{11} and D_{13} to find first the thermal ambipolar diffusion coefficients and the corresponding radial electric field and then the respective bootstrap current. This is made taking experimental density and electron and ion temperature profiles. In spite of the convergence problems of DKES at low collisionality, we can obtain bootstrap current values with acceptable uncertainties, without using Monte Carlo methods. The resulting rotational transform is used to obtain the rational surfaces' location and predict the transport barriers observed in the experiments.

1. Introduction

Transport theory in plasmas provides a way to determine the transport coefficients that enter in the linear relations between fluxes and thermodynamic forces, valid for relatively small gradients. The kinetic equation at the microscopic level is used to obtain these macroscopic relations, which represent common phenomenological observations, such as Fick's or Fourier's laws. The generalized formulation in a magnetically confined plasma provides the flux-surface-averaged particle, electron and ion energy cross-field fluxes, as functions of the radial gradients of particle density, electron temperature, ion temperature and electric potential. In neoclassical collisional transport of toroidally confined plasmas, the proportionality coefficients can be computed as functions of the magnetic configuration, plasma collisionality and radial electric field.

An analogous equation can also be found for the bootstrap current, which is a field aligned current due to neoclassical effects produced by trapped particles (*1*). This appears when there are temperature and density radial gradients, which give rise to a net trapped particle current, which is then collisionally transferred to circulating particles. The

---

coefficients of the radial gradients can be computed from kinetic theory and depend on the magnetic configuration, collisionality and electric field. The bootstrap (BS) current has been proposed as a means to achieve non-inductive operation of a tokamak. In current-less stellarators, its presence is not desired since it can modify the confining field produced by external conductors. But in some cases the bootstrap current can be used to alter the rotational transform profile and attain improved confinement regimes in stellarators (*2*, *3*).

Our interest here is to obtain the BS current in stellarators, where it is usually considered not to be so important. Computations of the BS current can be done in approximate ways using neoclassical theory, leading to analytical expressions (*4*, *5*), which, however, have limited validity. More accurate computations have to be done numerically, solving the drift kinetic equation. In solving this equation, there are two numerical methods that have traditionally been used: (1) a variational principle that minimizes the entropy production (DKES code (*6*)) and (2) Monte Carlo simulations (*7*). Both methods run into difficulties in the long mean free-path regime; DKES does not converge well and MC codes take extremely long times, which scale as a larger-than-one power of the mean free-path. Some improvements in performance with MC simulations at low collisionality have been achieved with the use of the so-called δf methods (*8*). These procedures have been applied to compute the bootstrap current in different stellarators and used to make inter-machine comparisons (*8*). Also, for the TJ-II heliac, the bootstrap current was computed using model density and temperature profiles for low- and high-density regimes by means of MC and DKES (*9*). In all these calculations, the magnetic geometry is fixed and it does not include the presence of the BS current that is being computed. In the present paper we devote to obtain the BS current in a self-consistent way, i.e. computed from a magnetic equilibrium that includes the BS current itself. For that, we start from the vacuum magnetic field and after obtaining the BS current we recompute the equilibrium and iterate the process until self-consistency is attained. We focus on the use of DKES code, although the low collisionality regime is not accurately represented, but we estimate the error bars. Even though the bootstrap current cannot be easily measured, we compare the results with an indirect experimental estimate of the rotational transform.

2. The TJ-II experiment

The TJ-II flexible Heliac is a stellarator having a helical magnetic axis that winds around a circumference of radius $R_0 = 1.5$ m. The plasma has a bean-shaped cross section with average minor radius of $a \approx 0.2$ m and magnetic field at the axis $B_0 \approx 1$ T. The plasmas are initiated with Electron Cyclotron resonance Heating (ECH); the absorbed heating powers are normally $P_{ECH} = (200 - 400)$ kW and in the absence of other heat sources the line-averaged densities are $n = (0.3 - 1.0) \times 10^{19}$ m^{-3} with central electron temperatures $T_e(0) \sim 1$ keV and ion temperatures $T_i(0) \sim 0.1$ keV coming from collisional heat exchange. Additional heating and fueling can be obtained with the help of one or two neutral beam injectors (NBI) delivering port-through powers $P_{NBI} = (300 - 700)$ kW each. For line densities above about 1.2×10^{19} m^{-3}, the ECH is no longer effective and the plasmas are sustained with NBI heating alone up to densities $n = (2.0 - 6.0) \times 10^{19}$ m^{-3} with lower temperatures: $T_e(0) \leq 0.3$ keV and $T_i(0) \sim 0.5 T_e(0)$. The electron density and temperature profiles are measured using the Thomson Scattering diagnostic from the magnetic axis up to $\rho \approx 0.7$, where ρ is the normalized flux surface label proportional to the square root of the enclosed

plasma volume. In order to obtain the density profiles, atomic beam, interferometry and reflectometry data are used to extend the profiles to the edge, ensuring that their line integral matches the experimental value. The ion temperature is normally measured with the CX neutrals analyzer. $T_i(\rho)$ is quite homogeneous in the low-density ECH plasmas and thus very different from T_e profiles due to the low collisional coupling in these cases.

It has been found that there is a close connection between the location of low-order rational magnetic surfaces and transport barriers in TJ-II (*10*). This fact can be used to pin down the precise location of a given rational surface by determining the experimental profile of the heat conductivity and finding the radii where it has local minima. This is obtained from the density and temperature profiles and computing the electron heat conductivity from local energy balance: $\chi_e = Q_e/(n_e \, dT_e/d\rho)$, where $Q_e = \int^\rho P_e \, d\rho$ is the integrated total power density deposited in the plasma (ECH or NBI) up to radius ρ. 2D maps of the effective heat diffusivities χ_e obtained in this way have been computed as function of radius and deposited power (*3*, *11*). Based on these, the radial positions where χ_e is minimum can be clearly seen, which may be identified with a low-order rational surface. We use this information to check the contribution of the bootstrap current to the rotational transform profile.
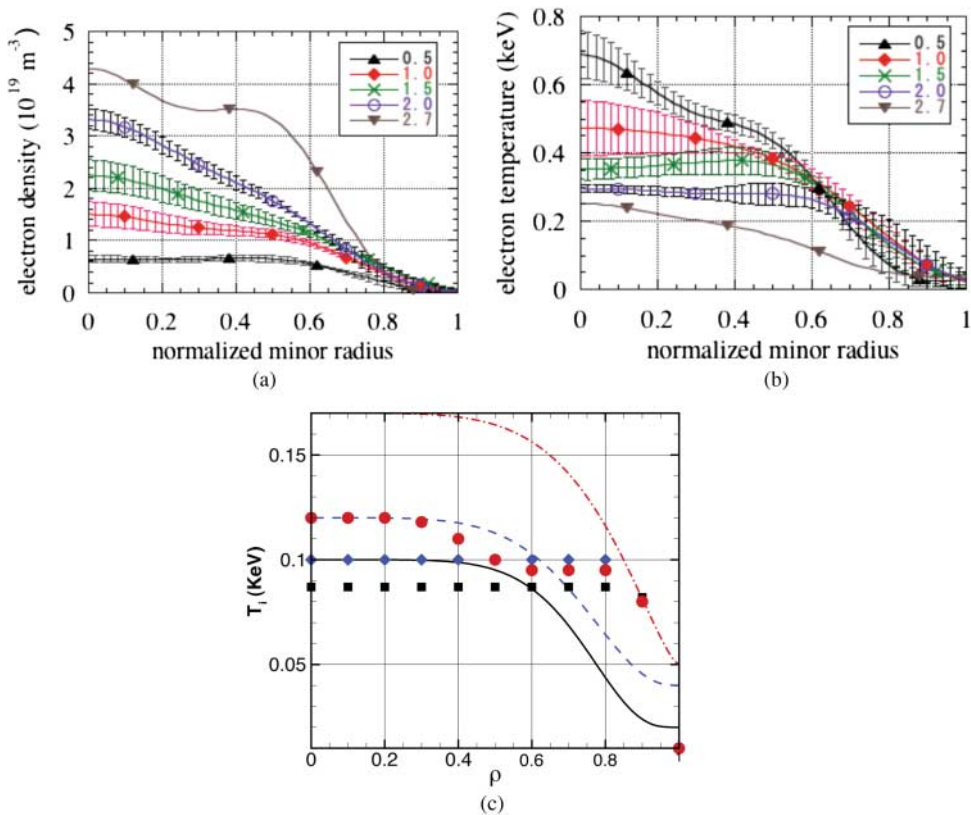

Figure 1. Averaged profiles over several discharges with the same line-averaged density, for five densities (in units of 10^{19} m^{-3}). (a) Density and (b) electron temperature profiles. (c) Ion temperature profiles for three line densities (low, medium and high).

The discharges used in the present analysis have no induced plasma current so that all the current is due to bootstrap. The magnetic configuration considered is the 100_44_64, meaning that the helical coil current is 4.4 kA (while central and vertical coils have 10 and 6.4 kA). Measured density and temperature (ion and electron) profiles for several TJ-II discharges in this configuration were used for a given line-averaged density value to obtain averaged profiles. Thus, characteristic profiles for each line density were obtained, ranging from low $n \sim 0.5 \times 10^{19}$ m^{-3} (ECRH) to high $n \sim 2.7 \times 10^{19}$ m^{-3} (NBI). These are shown in Figure 1 and represent the profiles used in all the computations that follow.

3. The bootstrap current and neoclassical transport

The linear relationship between radial fluxes and thermodynamic forces obtained from neoclassical theory, for each species $b = e, i$, is given by

$$\langle \vec{\Gamma}_b \cdot \nabla r \rangle = -L_{11} \left(\frac{1}{n} \frac{dn}{dr} - Z_b e \frac{E_r}{T_b} - \frac{3}{2T_b} \frac{dT_b}{dr} \right) - L_{12} \frac{1}{T_b} \frac{dT_b}{dr}, \tag{1}$$

$$\frac{\langle \vec{j}_b \cdot \vec{B} \rangle}{q_b B} = -L_{31} \left(\frac{1}{n} \frac{dn}{dr} - Z_b e \frac{E_r}{T_b} - \frac{3}{2T_b} \frac{dT_b}{dr} \right) - L_{32} \frac{1}{T_b} \frac{dT_b}{dr}. \tag{2}$$

The transport coefficients L_{ij} are obtained from mono-energetic coefficients D_{ij} by taking the average over the thermal distribution of energy. For a Maxwellian distribution this is

$$L_{ij} = \frac{2}{\sqrt{\pi}} \int_0^\infty K^{1/2} e^{-K} g_1 g_j D_{ij}(K) \, dK. \tag{3}$$

The coefficients $D_{ij}(K)$ are computed from the drift kinetic equation in the particular TJ-II magnetic geometry. They are functions of collisionality and the radial electric field in the local magnetic field. Here we use DKES (Drift Kinetic Equation Solver) code (6) to find the mono-energetic coefficients.

Equation (2) gives the bootstrap current, which is proportional to density and temperature gradients and also to the radial electric field E_r. The corresponding coefficients can both be computed from the mono-energetic coefficient D_{13} since $D_{23} = D_{13}$. Likewise, $D_{12} = D_{11}$, so that all the needed L_{ij}s can be obtained from the two D_{11} and D_{13}.

The first step is to get the equilibrium field for the given configuration 100_44_64. This is obtained from the VMEC code, providing the external boundary condition. Once the magnetic geometry is known, the mono-energetic coefficients D_{ij} are computed for each radial position in a chosen mesh with DKES. This was made for a range of collisionalities $(3 \times 10^{-5} - 300)$ and radial electric fields $(0 - 3 \times 10^{-2})$ spanning the relevant intervals. The numerical integrals in Equation (3) to find the thermal coefficients L_{ij} have to be done with a large enough upper limit (instead of infinity), which is dependent on E_r and ν^*, thus care must be taken to account for the proper ranges. In these computations, the profiles of $n(r)$ and $T_j(r)$ shown in Figure 1 were used for the various line densities plotted.

The resulting bootstrap current for each density is then introduced in the VMEC computation in order to get the updated MHD equilibria (one for each density).

DKES is used again and the cycle is repeated to obtain updated BS currents (for each density). This process is iterated until the BS current does not change any more. Convergence typically reached in two iterations.
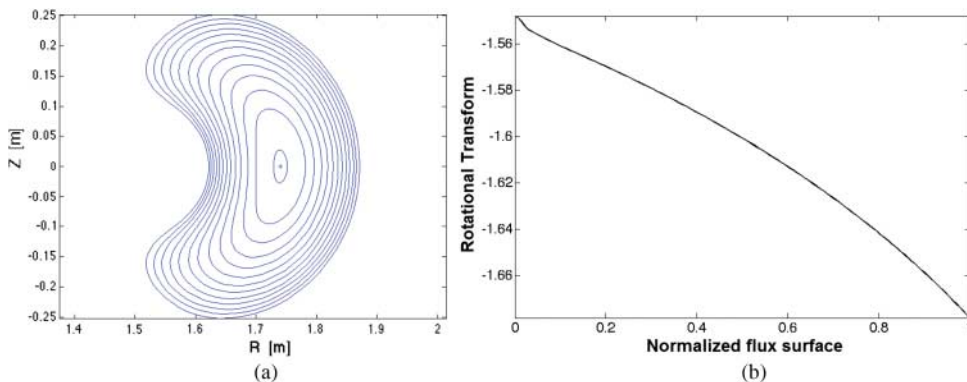
Figure 2. (a) Poloidal cross section of TJ-II magnetic surfaces for 100_44_64 configuration obtained from VMEC. (b) Vacuum rotational transform.

An important part of the procedure is the computation of the radial electric field. For calculating the BS current, the local value of E_r is needed and this is obtained from the ambipolarity condition:

$$\Gamma_i(E_r) = \Gamma_e(E_r).$$

Therefore, particle fluxes for electrons and ions as functions of the radial electric field have to be determined. This is made when D_{11} is obtained from DKES. The analysis of the neo-classical estimates of E_r with various approximations has been performed in (*12*), where it is shown that the E_r profiles obtained with DKES are similar to those from other simpler models. The coefficients D_{11} are thus used to compute $\Gamma_j(E_r)$ and afterwards D_{31} is used to compute $\langle j \cdot B \rangle$.

For the initial iteration, mono-energetic coefficients D_{ij} are computed for each radial position in a grid $\rho = (0.03, 1.0)$ with $\Delta\rho = 0.05$, using a starting VMEC equilibrium cor-responding to the vacuum rotational transform. The typical magnetic surfaces for this equilibrium are shown in Figure 2(a), while the $\iota(\rho)$ profile is displayed in Figure 2(b).

3.1. Mono-energetic coefficients

In Figure 3 the two mono-energetic coefficients, D_{11} and D_{13}, given by DKES are presented as function of collisionality, ν^*, for all the electric field values, E_r, considered. These corre-spond to the particular radius $\rho = r/a = 0.5$, but the behavior for all other radii is similar. The first iteration shown here was done with a not-so-large number of harmonics for the magnetic equilibrium, in order to reduce the computation time. For that reason there are large errors at low ν^*, shown with the bars, due to the poor convergence of the variational method.

The coefficient D_{11} as function of collisionality shows the behavior $1/\nu$ for low E_r typical of stellarators at low ν. Also, for intermediate ν the plateau regime is appreciated while for high ν the neoclassical Pfirsch–Schluter regime proportional to the collision frequency can be seen. At larger E_r the regime $\sqrt{\nu}$ appears at the smallest collisionalities. The results for D_{31} are consistent with previous results obtained using Monte Carlo simulations (*7*, *9*) for the same machine and are similar to those reported for other stellarators (*8*). In particular, it
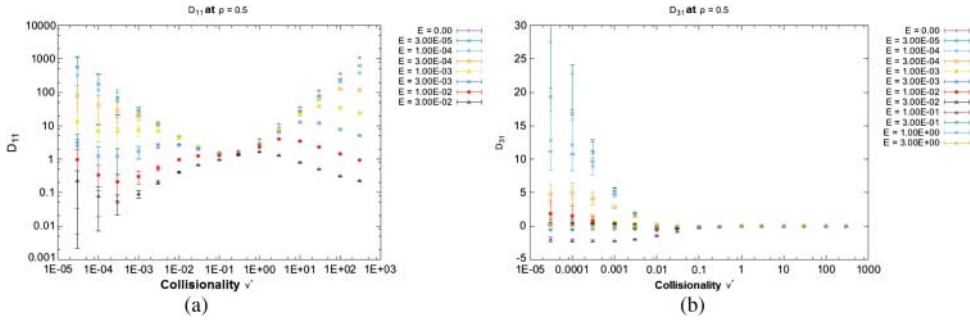
Figure 3. Mono-energetic coefficients for fluxes, D_{11}, and BS current, D_{13}, as function of collisionality for different values of the normalized radial electric field E_r, given in the legends. First iteration.
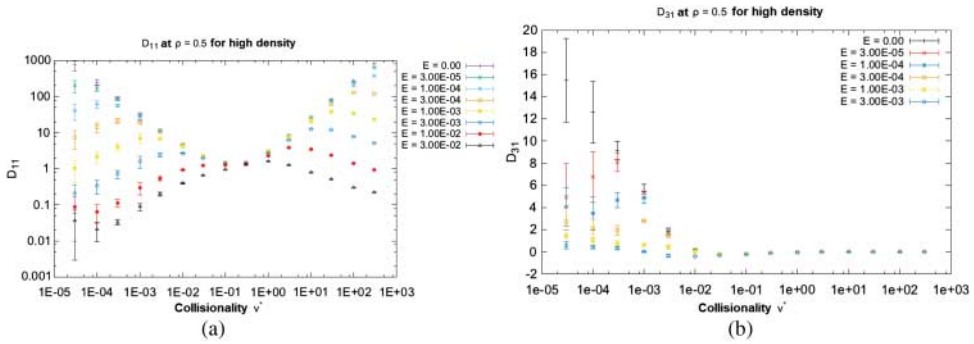

Figure 4. Mono-energetic coefficients for fluxes, D_{11}, and BS current, D_{13}, for a high-density case as function of collisionality and the normalized radial electric field. This second iteration has smaller error bars.

becomes very small for large collsionality since in this range there are no trapped particles to drive the bootstrap current.

The corresponding thermal coefficients L_{ij} are computed for each of the line-density values of Figure 1, and the BS current is derived as explained in the previous section. For each density, new VMEC equilibria are obtained which include the presence of the BS current. They are in turn used for DKES computations to obtain the D_{ij} coefficients, but for this second iteration the coupling order for DKES is increased to reduce errors at low ν^*, i.e. the number of modes included to describe the magnetic field is doubled. The coefficients for a mid-radius ($\rho = r/a = 0.5$) for the case of high line density are shown in Figure 4. As it is evident, smaller errors result at low ν^*.

3.2. Ambipolar electric field

To include the effect of the radial electric field on the transport and on the associated BS current, the E_r has to be computed using the particle fluxes Γ_j obtained from mono-energetic coefficients D_{11}. The ambipolar condition $\Gamma_i(E_r) = \Gamma_e(E_r)$ determines the E_r field. This equation can have up to three roots, one of them is unstable. When two roots are possible, the criterion to choose the right root is based on heat production minimization. The
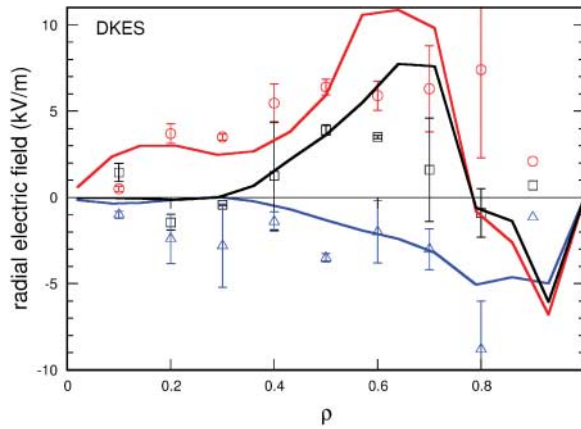
Figure 5. Radial electric field profiles computed from ambipolarity condition for three densities: low (red), medium (black) and high (blue). Experimental values are also shown with the symbols.

profiles obtained in this way can be seen in Figure 5 for three densities. The experimental values of E_r are shown with the symbols, obtained from heavy ion beam probe (HIBP) diagnostics (12). These are the E_r profiles used to compute the BS current.

4. Results for the bootstrap current

In first iteration the resulting BS current is different for each of the average densities considered. In Figure 6(a) the resulting current for the low line-averaged density $n = 0.5 \times 10^{19}$ m^{-3} is shown, while Figure 6(b) presents the current for the highest density $n = 2.5 \times 10^{19}$ m^{-3}. Ion and electron currents are shown separately and the total current is represented with the lines. The larger density has larger BS current for the profiles used here. The electron current is generally dominating over the ion current because the electron temperature is always larger that the ion temperature. Larger T_e means lower ν and consequently larger values of D_{31}.
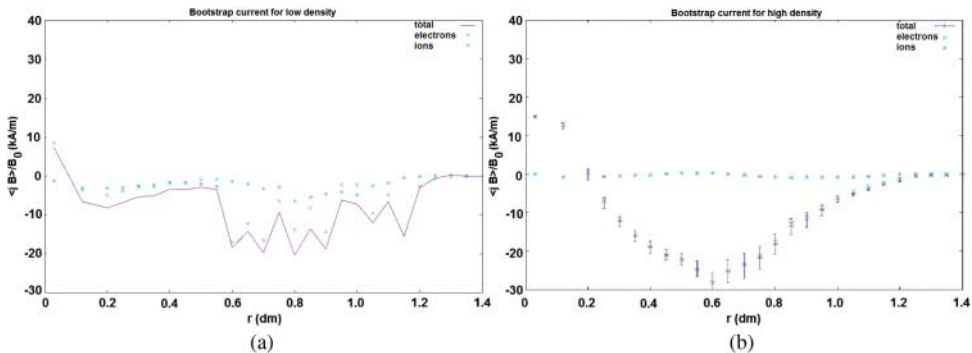

Figure 6. Bootstrap current profiles for the first iteration for the low (a) 0.5×10^{19} m^{-3} and high (b) 2.5×10^{19} m^{-3} line-averaged densities. Electron, ion and total currents can be seen.

These profiles are input to VMEC to get one magnetic equilibrium from each density and each one is used to obtain the D_{ij}s already shown in Figure 4. In the second iteration, the resulting BS current for each average density is already self-consistent, in the sense that the VMEC equilibria obtained with the new BS current are not distinguished from the previous ones. These final BS current profiles are shown in Figure 7 for the low-, medium- and high-density cases. The corresponding error bars due to the poor convergence are shown.

For low densities, a discontinuity close to the middle radius is observed, producing a sign change followed by and increment in the total current. This behavior is also qualitatively observed in other computations (7, 9). It is worth mentioning that the DKES calculations use the Lorentz collision operator, which does not conserve momentum; thus, a momentum conserving correction should be applied as explained in (13), which has the effect of increasing the ion current contribution. Then the total BS current decreases but the profile shape is similar. For this reason, the values obtained here for the BS current are larger than those found in previous works. The total BS current is obtained integrating over the plasma cross section; the values obtained for the low, medium and high densities are $I_{BS} = 4.2$, 7.6 and 5.5 kA, respectively. These values are somewhat high.

4.1. Rotational transform

Adding the BS current to the coil currents the total self-consistent rotational transform for each density is obtained. Since the BS currents found have a non-monotonic behavior, the
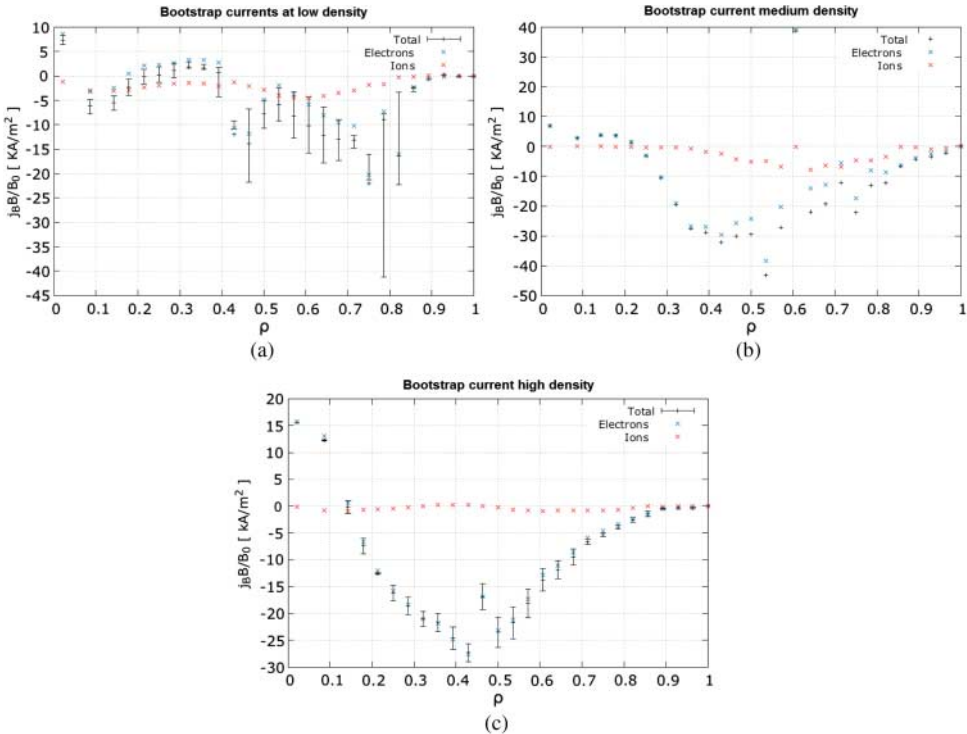

Figure 7. Self-consistent bootstrap current profiles for electrons $j_{bs,e}$, ions $j_{bs,i}$ and total $j_{bs} = j_{bs,e} + j_{bs,i}$, for the low (a), medium (b) and high (c) line-averaged densities.
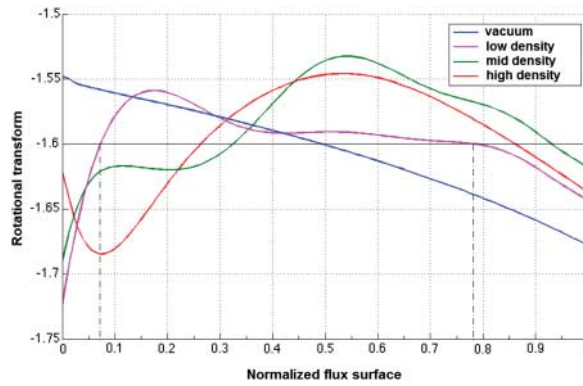
Figure 8. Rotational transform profiles for initial state (no BS current, vacuum fields) and with the inclusion of the BS currents for the three line-averaged density regimes. Notice the small variation range in ι.

$\iota(r)$ profile behaves the same way having minima and maxima at certain radii, as can be seen in Figure 8. Low-density values correspond to ECRH plasmas and the high-density case is for plasma heated by NBI.

Since there are no measurements of the rotational transform in TJ-II, we can try to have some information about it from some indirect results, so we can compare our estimates with real data.

As mentioned in Section 2, low-order rational surfaces have been found to be the sites of transport barrier formation in TJ-II. The electron thermal conductivity can be obtained experimentally by $\chi_e = Q_e/nT_e'$ from measurements of $n(r)$ and $T_e(r)$ profiles and the injected ECRH power $P_{ECH,e}$ (in low-density plasmas). A rational surface should then be located at the radius where χ_e is low, and that should agree with the ι profile. In (14) a scanning of the helical current was made in order to vary the ι profile in ECH plasmas (low density). The values of χ_e were computed and the χ_e radial profiles were plotted as function
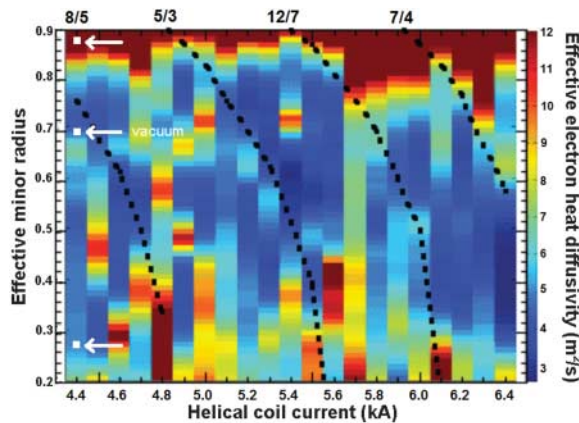

Figure 9. Electron thermal conductivity χ_e values (in right-side scale) as function of radius and helical current, obtained when a scanning of the helical current was produced. Arrows show location of rational surface $\iota = 8/5$ without (vacuum) and with BS current.

of the helical current, as shown in Figure 9. For the configuration 100_44_64, we are considering, $I_{hc} = 4.4$ kA. Thus, the leftmost area of the plot gives the (χ_e/ρ) profile. The low-order rational within the range of ι is $\iota = 8/5$. According to Figure 8, there are two radii where $\iota = 8/5$ for the low-density regime, in contrast to the vacuum rotational transform, which has a single value at about $\rho = 0.7$. The location of the rational close to the edge is actually quite ambiguous since the profile in that region is very flat and a slight variation in the value of $\iota(\rho)$ can change the radius of the rational $\rho_{8/5}$. The white arrows in Figure 9 show the locations of the 8/5 rational. As can be seen, the small-ρ rational coincides with a low diffusivity region (blue); the large-ρ rational does not but this is subject to the uncertainties just mentioned.

5. Conclusions

- A self-consistent computation of the bootstrap current in the TJ-II stellarator was presented using DKES code finding values relatively higher than other calculations (*7*, *9*, *15*).
- Large uncertainties at low collisionalities are part of the reason. This is reduced by increasing the number of terms in the representation of *B*-field, but very long CPU times are required. DKES computations have been complemented by Monte Carlo methods in other works (*9*). This was not attempted here.
- Momentum conservation of the collision operator in the drift kinetic equation could be imposed to improve the results (*13*).
- The non-monotonic ι profile for ECRH heating can explain two regions of reduced transport in TJ-II, when the relation between transport barrier and low-order rationals found in TJ-II (*10*) is used.
- The general results agree with results in other machines (*8*, *16*).

Disclosure statement

No potential conflict of interest was reported by the authors.

References

(1) Helander, P.; Geiger, J.; Maaßberg, H. *Phys. Plasmas* **2011,** *18*, 092505.
(2) López-Bruna , D.; Estrada, T.; Medina, F.; de la Luna, E.; Romero, J.A.; Ascasíbar, E.; Casteón, F.; Vargas, V.I. *EPL* **2008,** *82*, 65002.
(3) Vargas, V.I.; López-Bruna, D.; Herranz, J.; Casteón, F. *Nucl. Fusion* **2007,** *47*, 1367.

(4) Shaing, K.C.; Carreras, B.A.; Dominguez, N.; Lynch, V.E.; Tolliver, J.S. *Phys. Fluids B: Plasma Phys.* **1989,** *1*, 1663.

(5) Sugama, H.; Nishimura, S. *Phys. Plasmas* **2002,** *9*, 4637.

(6) Hirshman, S.P.; Shaing, K.C.; van Rij, W.I.; Beasley, C.O.; Crume, E.C. *Phys. Fluids* **1986,** *29*, 2951.

(7) Tribaldos, V.; Beidler, C.D.; Turkin, Y.; Maaßberg, H. *Phys. Plasmas* **2011,** *18*, 102507.

(8) Beidler, C.D.; Allmaier, K.; Isaev, M.Yu.; Kasilov, S.V.; Kernbichler, W.; Leitold, G.O.; Maaßberg, H.; Mikkelsen, D.R.; Murakami, S.; Schmidt, M.; Spong, D.A.; Tribaldos, V.; Wakasa, A. *Nucl. Fusion* **2011,** *51*, 076001.

(9) Velasco, J.L.; Allmaier, K.; López-Fraguas, A.; Beidler, C.D.; Maaßberg, H.; Kernbichler, W.; Castejón, F.; Jiménez, J.A. *Plasmas Phys. Control. Fusion* **2011,** *53*, 115014.

(10) López-Bruna , D.; Pedrosa, M.A.; Ochando, M.A.; Estrada, T.; van Milligen, B.P.; López-Fraguas, A.; Romero, J.A.; Baião, D.; Medina, F.; Hidalgo, C.; Ascasíbar, E.; Pastor, I; Rodríguez, C; Tafalla, D. *Plasma Phys. Control. Fusion* **2011,** *53*, 124022.

(11) Tallents, S.; López-Bruna, D.; Velasco, J.L.; Ochando, M.A.; Van Milligen, B.P.; Vargas, V.I.; Martinell, J.J.; Tafalla, D.; Fontdecaba, J.M.; Herranz, J.; Blanco, E.; Tabarés, F.L.; Estrada, T.; Pastor, I. *Plasma Phys. Control. Fusion* **2014,** *56*, 075024.

(12) Gutiérrez-Tapia , C.; Martinell, J.J.; López-Bruna, D.; Melnikov, A.V.; Eliseev, L.; Rodríguez, C.; Ochando, M.A.; Castejón, F.; García, J.; van Milligen, B.P.; Fontdecaba, J.M. *Plasma Phys. Control. Fusion* **2015,** *57*, 115004.

(13) Maaßberg , H.; Beidler, C.D.; Turkin, Y. *Phys. Plasmas* **2011,** *16*, 072504.

(14) López-Bruna, D.; Vargas, V.I.; Romero, J.A. *J. Phys. Conf. Ser.* **2015,** *591*, 012013.

(15) Tribaldos V.; Maaßberg H.; Jiménez J.A.; Varias A. 30th EPS Conference, St. Petersburg, ECA, 27A, 2003, P1.28.

(16) Watanabe, K.; Nakajima, N.; Okamoto, M.; Nakamura, Y.; Wakatani, M. *Nucl. Fusion* **1992,** *32*, 1499.